

Copper Nanoparticle Sintering Enabled Hermetic Packaging With Fine Sealing Ring for MEMS Application

Hu, Dong; Shah, Mustafeez Bashir; Fan, Jiajie; Vollebregt, Sten; Zhang, Guoqi

DOI

[10.1109/TED.2023.3312066](https://doi.org/10.1109/TED.2023.3312066)

Publication date

2023

Document Version

Final published version

Published in

IEEE Transactions on Electron Devices

Citation (APA)

Hu, D., Shah, M. B., Fan, J., Vollebregt, S., & Zhang, G. (2023). Copper Nanoparticle Sintering Enabled Hermetic Packaging With Fine Sealing Ring for MEMS Application. *IEEE Transactions on Electron Devices*, 70(11), 5818 - 5823. <https://doi.org/10.1109/TED.2023.3312066>

Important note

To cite this publication, please use the final published version (if applicable). Please check the document version above.

Copyright

Other than for strictly personal use, it is not permitted to download, forward or distribute the text or part of it, without the consent of the author(s) and/or copyright holder(s), unless the work is under an open content license such as Creative Commons.

Takedown policy

Please contact us and provide details if you believe this document breaches copyrights. We will remove access to the work immediately and investigate your claim.

Green Open Access added to TU Delft Institutional Repository

'You share, we take care!' - Taverne project

<https://www.openaccess.nl/en/you-share-we-take-care>

Otherwise as indicated in the copyright section: the publisher is the copyright holder of this work and the author uses the Dutch legislation to make this work public.

Copper Nanoparticle Sintering Enabled Hermetic Packaging With Fine Sealing Ring for MEMS Application

Dong Hu¹, Member, IEEE, Mustafeez Bashir Shah², Jiajie Fan, Senior Member, IEEE, Sten Vollebregt³, Senior Member, IEEE, and Guoqi Zhang⁴, Fellow, IEEE

Abstract—Driving by the increased demand for hermetic packaging in the more than Moore (MtM) roadmap, a Cu nanoparticle sintering-enabled hermetic sealing solution was developed with a small-size sealing ring. The developed technology simplifies microfabrication and requires less surface roughness using a sinterable Cu nanoparticle paste. A 50 μm size Cu paste sealing ring was achieved using a lithography patterned photoresist as a stencil mask. A groove-structured chip was used to amplify localized stress. The Cu nanoparticle paste was fully sintered at 300 °C under pressure ranging from 10 to 40 MPa resulting in a robust bonding with a maximum shear strength of 280 MPa and implementing hermetic packaging. The deflection of the Si diaphragms estimated a vacuum level of 7 kPa. Vacuum sealing was maintained for over six months, and the lowest leak rate was calculated as $8.4 \times 10^{-13} \text{ Pa} \cdot \text{m}^3/\text{s}$. The developed technology that comprises small-size patterning and pressure-assisted sintering offers the potential for a simple, cost-effective, but robust solution for hermetic packaging.

Index Terms—Cu nanoparticle, hermetic packaging, leak rate, pressure-assisted sintering.

I. INTRODUCTION

IN THE concept of more than Moore (MtM), the non-digital functions, including RF, power and sensors, will be the focal point of future commercial prospects [1]. Notably, microelectromechanical systems (MEMSs) often require a hermetic environment to realize the appropriate sensitivity and performance. In addition, capping the sensitive components in a vacuum environment guarantees their reliability. On the path to a high integration density on a single chip, a cost-effective and precise hermetic packaging solution for MEMS sensors is a significant challenge.

Manuscript received 2 May 2023; revised 11 August 2023; accepted 31 August 2023. Date of publication 14 September 2023; date of current version 24 October 2023. This work was supported by the ECSEL Joint Undertaking (JU) under Grant 826417. The JU receives support from the European Union's Horizon 2020 research and innovation program and Germany, Austria, Spain, Finland, Hungary, Slovakia, Netherlands, Switzerland. The review of this article was arranged by Editor D. J. Young. (Corresponding author: Guoqi Zhang.)

The authors are with the Laboratory of Electronic Components, Technology and Materials (ECTM), Department of Microelectronics, Delft University of Technology, 2628 CD Delft, The Netherlands (e-mail: g.q.zhang@tudelft.nl).

Color versions of one or more figures in this article are available at <https://doi.org/10.1109/TED.2023.3312066>.

Digital Object Identifier 10.1109/TED.2023.3312066

As a critical part of hermetic packaging, the bonding technology can be categorized by the presence or absence of an intermediate layer bonding [2]. The bonding technology without an intermediate layer comprises anodic bonding and direct bonding. The process involves high voltage and high temperature (>1000 °C), respectively, which pose challenges to the stability of components [3], [4]. The bonding technology with an intermediate layer can also be divided into a non-conductive intermediate layer, such as glass frit bonding [5], and a conductive metal-based intermediate layer.

Metallic bonding techniques, as widely used in hermetic seal methods, include solder bonding, eutectic bonding, solid-liquid interdiffusion bonding (SLID), surface-activated bonding, and thermo-compression bonding. However, solder and eutectic bonding have disadvantages because the melting of solder alloys can cause reflow concerns. The sealing ring widths frequently exceed 100 μm in meeting the required hermeticity and bond strength [6], [7]. SLID bonding technique can result in the formation of voids in the intermetallic compound layer and therefore requires extra considerations, e.g., the sealing layer thickness and temperature profile [8]. Surface-activated bonding permits sealing at room temperature. However, substrates' surface planarity and roughness requirements are very stringent [9]. Thermo-compression bonding utilizes high temperature and pressure and has been demonstrated with metals like Al [10] and Cu [11].

Over the last decade, metallic nanomaterial sintering technology, represented by Ag and Cu, has been widely investigated in power electronics packaging because of the low process temperature and excellent stability at high operation temperature [12], [13], [14]. In addition, it also has been reported in the application of 3D-IC integration, e.g., chip-to-chip, wafer-to-wafer and wafer bonding, achieved by dip-transfer, and direct printing methods [15], [16], [17]. Recently, few attempts have been made to apply nanomaterial sintering in a hermetic package. It has been reported that sinterable Ag film can implement hermetic sealing through thermo-compression and electric-assisted sintering [18], [19]. However, the hermeticity degradation over time has not been reported, and the application of sinterable metal film increases the cost unless used as a fine sealing ring.

This study proposes a hermetic sealing solution using Cu nanoparticle sintering with a 50 μm size sealing ring. The sealing ring was patterned through lithographically defined

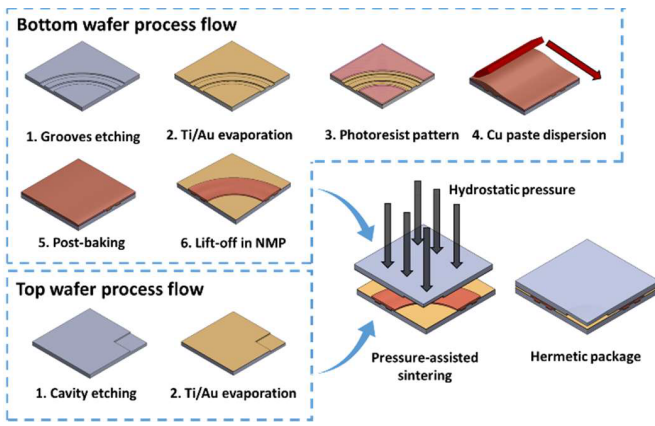


Fig. 1. Microfabrication process flow (one quadrant of the die is presented for better illustration).

stencil printing [20]. Hermeticity was achieved in a Si cavity on an Au-finished Si substrate. Multiple sintering profiles were studied to investigate the feasibility of hermeticity and bonding strength. Analysis of the fracture surface subsequently revealed the mechanism of hermeticity. Finally, the deflection of the Si diaphragm was recorded over six months, and a relatively low leak rate was demonstrated.

II. DESIGN AND MICROFABRICATION

A. Geometry Design

A simple two-chip test hermetic package was built for proof of concept (Fig. 1). A thin diaphragm with a dimension of 4×4 mm and thickness of $50 \mu\text{m}$ was created in the top component. Thus, the interior cavity pressure could be measured by its deflection. Furthermore, a groove structure was designed in the bottom component to create nonuniform stress over the sealing ring area. Locally amplified stress was therefore designed to promote nanoparticle sintering and eliminate the pores. Three parallel $5 \mu\text{m}$ width groove structures followed the geometry of a 5×5 mm square with rounded corners. The radius of the rounded corners was $250 \mu\text{m}$, and the intergroove spacing was $4 \mu\text{m}$.

B. Process Flow

Fig. 1 presents the process flow for microfabrication. According to the symmetric geometry, one quadrant of the die is presented for better illustration.

For the Si bottom wafer, a $2.5 \mu\text{m}$ deep designed groove structure was etched away by reactive ion etching. Following this was the growth of a 100 nm thermal oxide layer, which provides good adhesion for the metal layer. Afterward, a $20 \text{ Ti}/200 \text{ nm Au}$ layer was e-beam evaporated to strengthen the sealing ring–component interface. A $3.5 \mu\text{m}$ thick negative photoresist was coated with varying openings, followed by Cu nanoparticle paste (CP-005, Mitsui Mining and Smelting Company, Ltd., Japan) dispersion with a silicone squeegee. Subsequently, the sample was baked in the air at $80 \text{ }^\circ\text{C}$ for 5 min. This baking step evaporated organic solvent to promote the adhesion between the dried paste and the substrate. Eventually, the small-size paste pattern was formed by a lift-off process. The baked sample was bathed in $80 \text{ }^\circ\text{C}$ N-Methyl-2-pyrrolidone (NMP) solvent for 1 min to strip the photoresist.

The process of the top wafer contains mainly two steps. Deep reactive ion etching (DRIE) was employed to create a

$450 \mu\text{m}$ deep cavity, where a $5 \mu\text{m}$ plasma-enhanced chemical vapor deposition (PECVD) SiO_2 worked as the hard mask. Afterward, the same $20 \text{ Ti}/200 \text{ nm Au}$ layer was evaporated on the surface of the top wafer.

This study employed pressure-assisted sintering for the die-level metal-metal bonding in a vacuum wafer bonder (Applied Microengineering Ltd., U.K.) The dies were manually aligned with each other. The sintering temperature from $275 \text{ }^\circ\text{C}$ to $350 \text{ }^\circ\text{C}$ was performed, whereas the pressure ranged from 1.5 to 40 MPa. A constant sintering time was controlled at 10 min. A low-pressure (0.1 kPa) $5\% \text{ H}_2/\text{N}_2$ forming gas was inserted during the first 5 min of sintering to reduce the oxide. A high vacuum $<0.01 \text{ Pa}$ was kept for the rest of the process, including the cooling phase.

C. Hermeticity Evaluation

The evaluation of the hermeticity of the sample was achieved by monitoring the pressure-driven deflection of the diaphragm using an optical profilometer. If the sample is successfully sealed, the diaphragm deflects due to the pressure difference between the interior and exterior of the cavity.

Diaphragm deflection (δ) determines the pressure difference (ΔP) between the inside and outside of the package. Equation (1) illustrates the relationship between the diaphragm deflection and the pressure difference [21]

$$\Delta P = \frac{\delta E d^3}{a x^4} \quad (1)$$

where E is Young's modulus of silicon, d is the diaphragm thickness; a is the shape constant equal to 0.0138 when the diaphragm is square-shaped, and x is the diaphragm length.

By measuring the change in diaphragm deflection over time, the stability of the hermetic package can be determined using this method. If the package has a slight leak, the deflection will progressively decrease until the internal and external pressures of the cavity are equalized. The deflection at the center of the diaphragm is proportional to the differential pressure, and the leak rate L can be calculated using (2) [22]. The calculated leak rate includes the influence caused by nanoparticles outgassing during storage

$$L = \ln\left(\frac{W_{t1}}{W_{t2}}\right) \left(\frac{V P_0}{t_2 - t_1}\right) \quad (2)$$

where W_{t1} and W_{t2} are the maximum deflections at the center of the diaphragm at times t_1 and t_2 , respectively; P_0 is the ambient pressure outside the cavity, and V is the volume of the cavity.

III. RESULTS AND DISCUSSION

A. Formation of the Sealing Ring

Fig. 2 shows the Cu paste ring with a clean surrounding surface after the lift-off process. The width was kept around $50 \mu\text{m}$ as designed in the lithographic mask. Furthermore, the Cu paste ring's profile in two directions was measured. The highest point of the two cross sections is 2.2 and $2.09 \mu\text{m}$, respectively. The direction of stencil printing can influence the deviation of the ring height. It is noticed that the value is smaller than the photoresist height of $3.5 \mu\text{m}$, which is caused

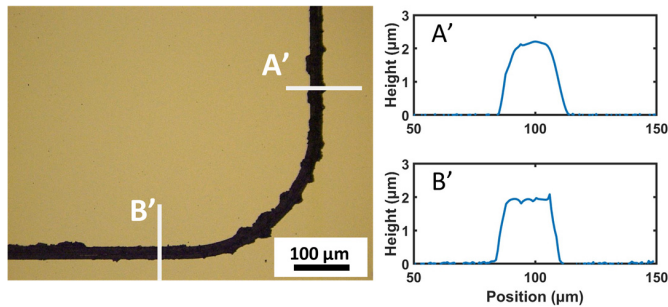


Fig. 2. Profile of Cu paste ring after lift-off.

by the shrinkage during the baking process. Besides, a non-flat surface is revealed. This can be attributed to more volumetric loss when covering a groove.

The result demonstrates that the lithographic lift-off method applies to the viscous paste to form a small-size sinterable structure for further heterogeneous integration.

B. Evaluation of Bonding Strength

In general, low-temperature sintering of nanomaterials results in a porous structure, and the interparticle bonding highly relies on the sintering condition, temperature, pressure, and dwell time.

In this study, a design of experiments (DOEs) comprising sintering temperatures ranging from 275 °C to 340 °C and sintering pressure ranging from 1.5 to 40 MPa were conducted to explore the feasibility of realizing hermetic packaging. The results are scattered in Fig. 3. In all groups, the top die was successfully bonded with the bottom die through pressure-assisted sintering technology.

As a result, we found that the sample fabricated with a sintering temperature higher than 300 °C and pressure larger than 10 MPa could result in a deflected diaphragm, indicating a sealed vacuum chamber at 0 h. In contrast, the red region in Fig. 3 represents the non-vacuum sealable region. This region comprises the combination of temperatures <300 °C and applied pressure values of <10 MPa. Sufficient sintering temperature enables the surface diffusion between nanoparticles to promote the neck area. Sintering pressure, on the other hand, plays a crucial role in eliminating the pores and therefore reducing the porosity. Therefore, the softest sintering parameter to realize hermetic sealing was determined as 300 °C and 10 MPa.

Moreover, the bonding strength of the sample sintered at 300 °C was evaluated by the shearing test on a Royce 650 Universal Bond Tester, as shown in Fig. 4. To comprehensively assess the shear strength, each sample was diced into four quadrants using a standard dicing saw. The quadrants were glued on a leadframe for the shear test, as shown in the inserted frame in Fig. 4. Therefore, each data points represent the average value of four tests.

Except for the sample sintered at 1.5 MPa, the samples survived the mechanical dicing process. The shearing results are plotted in Fig. 4. The bonding area was theoretically calculated as 0.127 mm². The bonding strength increases according to a higher sintering pressure. The promotion of the bonding strength is significant when the sintering pressure increases from 5 to 20 MPa. The bonding strength at 5 MPa

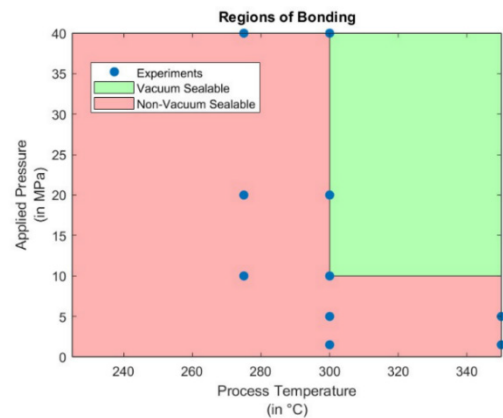


Fig. 3. Parameter study for the hermetic packaging.

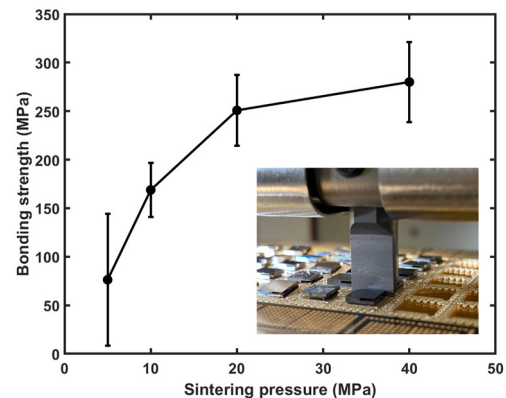


Fig. 4. Bonding strength with different sintering pressure.

sintering pressure is 76 MPa, which jumps to 250 MPa as the sintering pressure increases to 20 MPa. However, the improvement between the sintering pressure of 20 and 40 MPa is slight, as the bonding strength is 250 and 280 MPa, respectively.

Afterward, the fracture surface of a sample sintered at 300 °C and 10 MPa was analyzed, as shown in Fig. 5, to investigate the mechanism of hermeticity. Three typical morphologies can be found around the groove structure region. It can be seen that the microstructure in the grooves is porous, indicating insufficient sintering. In contrast, as shown in the insert, the surrounding microstructure is seamless and presents different contrast compared to the Au coating. The width of this light area is relatively 50 μm, which implies limited shrinkage along the horizontal direction. In addition, high structures were noticed remaining on the sealing ring area.

Energy dispersive X-ray (EDX) spectroscopy was used to identify the elements in the different structures, and the results of scanning on lines L1 and L2 are plotted in Fig. 5(c). The EDX results demonstrate that the non-flat high structure is purely Cu. Besides, the materials remaining in the grooves are also pure Cu. The surrounding structure contains a thin Cu layer.

To further investigate the porosity of the microstructure, the cross section of the failed groove structure was prepared by a focus ion beam (FIB), as shown in Fig. 6(a). Same as seen from the top surface, the internal microstructure of the thin Cu layer between grooves is also seamless. The Cu layer in the grooves, however, presents cracks and pores. This result is

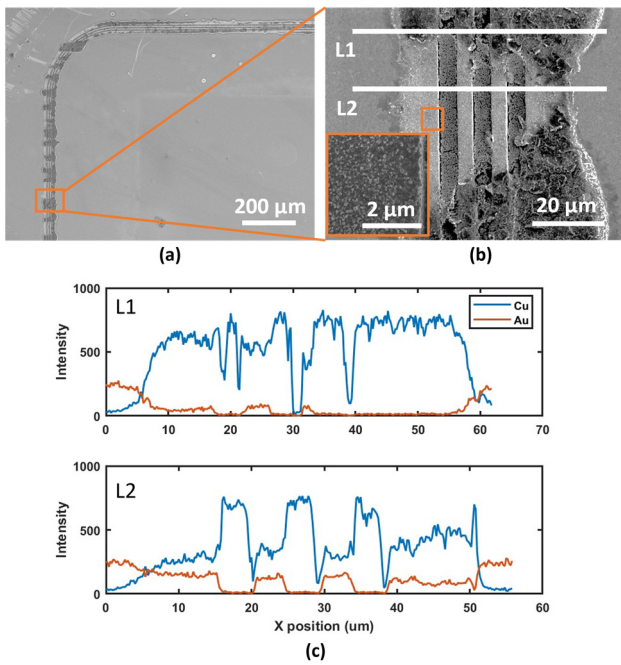


Fig. 5. Fracture surface of a sample sintered at 300 °C and 10 MPa. (a) Quadrant of the sealing ring. (b) Groove structures. (c) EDX line scan on the position marked in (b).

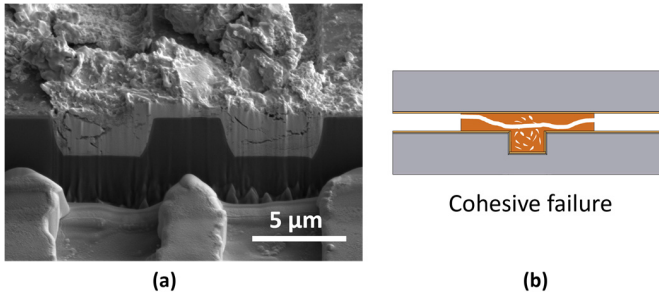


Fig. 6. (a) Cross section on the fracture surface. (b) Schematic of the failure.

consistent with the observed sealing ring morphology. The Cu paste layer was wave-shaped after lift-off (Fig. 2). The contact area between the top die and the Cu paste in the grooves was thus inadequate. Moreover, it had edges at these positions, leading to stress concentration.

The failure mode of the shear test can be identified as a cohesive failure [Fig. 6(b)] as negligible Au finish is exposed in the sealing ring area. The developed technology achieves hermeticity through the solid, seamless sintered Cu structure around the grooves, created using the amplified pressure at the edge of the patterned Cu structure.

C. Simulation of Hermeticity

To efficiently assess the vacuum level in the cavity, an FEA model was constructed in COMSOL Multiphysics. The Solid Mechanics module with Multiphysics coupling to the heat transfer in solids was applied. A quarter of the entire model was simulated due to its symmetry to save computational resources, as shown in Fig. 7. The simulation parameters adopted for each layer are listed in Table I. The properties of the bulk Cu were adopted for the sintered Cu paste structure.

The exterior boundary of the geometry was kept at a pressure of 1×10^5 Pa to emulate the atmospheric pressure. The

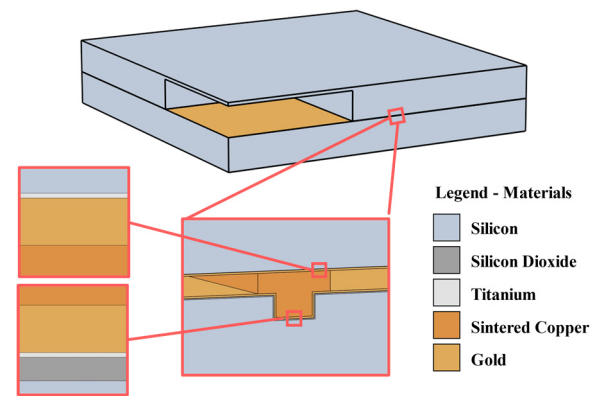


Fig. 7. Schematic of the FEA model.

TABLE I
SUMMARY OF MATERIAL PROPERTIES IN THE SIMULATION

Material	Young's modulus (GPa)	Poisson ratio	CTE ($10^{-6}/K$)	Thermal conductivity (W/mK)
Silicon	170	0.28	2.6	130
Gold	70	0.44	14.2	317
Titanium	115.7	0.321	8.6	21.9
Silicon dioxide	70	0.17	0.5	1.4
Sintered Cu paste	120	0.34	16.5	401

thickness of the diaphragm was determined as 50 μm. A parametric study was conducted with applied interior pressure ranging from 0 to 1×10^5 Pa. Furthermore, the temperature change during the sintering process was also considered in the simulation. The model was simulated from 300 °C down to 20 °C to incorporate the warpage effect caused by the CTE mismatch and geometry asymmetry, something which is not part of the analytical model.

The deflection in the diaphragm was successfully simulated with a low cavity interior pressure. The relationship between maximum deflection and interior cavity pressure from the FEM simulation and analytical model were plotted in Fig. 8, respectively. The inserted frame presents an example of surface displacement mapping when the interior cavity pressure was set as 1.6×10^{-3} Pa. The slope shows a slight deviation, which was caused by the selection of the shape constant. The FEA model simulated shape constant was 0.0156, while the analytical model adopted was 0.0138. It is because the deflected structure was not a perfect square. Therefore, the FEM model was verified with the analytical model. Additionally, the thermo-mechanical deformation causes residual deflection as the cavity is sealed at a high temperature.

D. Evaluation of Hermeticity

At first, the actual depth of the cavity was measured to calculate the pressure difference. Fig. 9 presents the profile of the Si cavity. The edge of the cavity is sharp, and the bottom surface is relatively flat. A 3-D visualization was inserted to show the high quality of DRIE. The thickness of the diaphragm before sintering activities was 78, 59, and 46 μm for the samples sintered under 10, 20, and 40 MPa, respectively.

Consistent with the simulation results, a deflected diaphragm was successfully formed after pressure sintering,

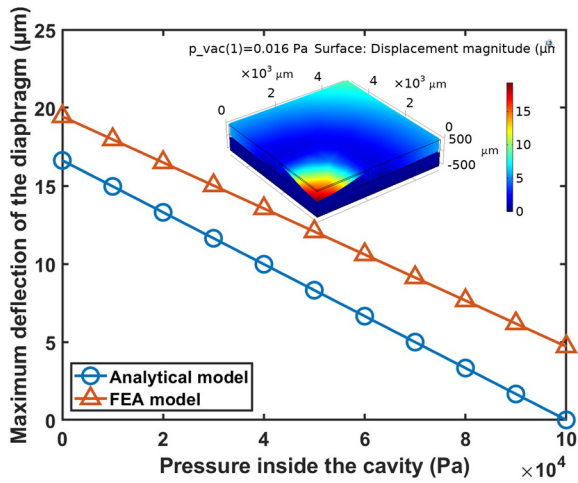


Fig. 8. Relationship between maximum deflection and interior cavity pressure with a 50 μm thickness diaphragm.

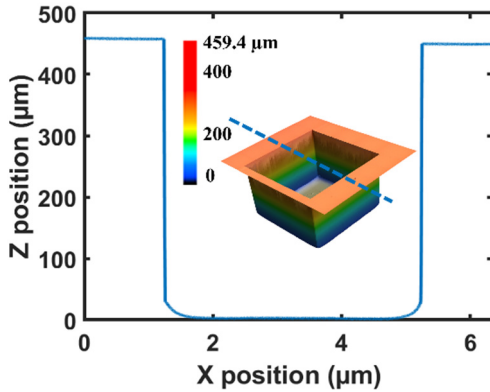


Fig. 9. 3-D profile of the etched cavity.

as shown in Fig. 10. In contrast, the non-vacuum-sealed sample shows a flat top surface as a reference. The symmetric deflection of the diaphragm is visualized with the top surface as the zero planes. The maximum displacement of the deflection is therefore determined as 12.3 μm .

With the known diaphragm thickness and the maximum deflection of the diaphragm, the sealed vacuum level can be calculated. The vacuum level for the sample sintered at 300 $^{\circ}\text{C}$ under 10, 20, and 40 MPa is 61.8, 60.0, and 7.2 kPa, respectively. There is no evidence to support the dependence of the cavity pressure on the sintering pressure. At the same temperature and sintering time, other influence factor could be the decomposed organic content in the paste composition, which is difficult to quantify.

It can be noticed that the sealed value is one to two orders higher compared to the forming gas pressure level (0.1 kPa) during the sintering. This increase could be attributed to the Cu paste materials composition. The organic solvent and binder decomposed during the bonding process and the decomposition products were therefore sealed in the cavity, resulting in a low-medium vacuum level.

The samples were stored at constant humidity and room temperature for around six months to assess the hermeticity. Fig. 11 presents the deflection evolution of the sample sintered under 10 MPa. The results reveal excellent vacuum stability of the sealed sample over 169 days. It can be seen that the

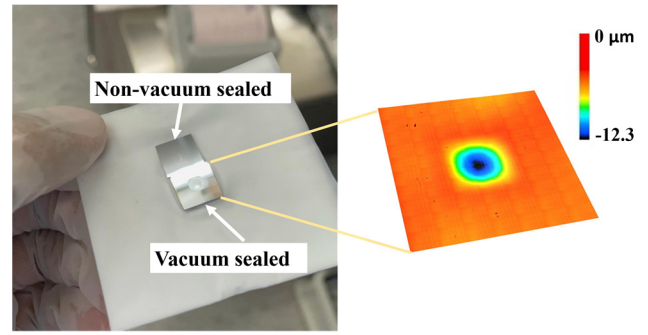


Fig. 10. Sample sintered at 300 $^{\circ}\text{C}$ under 10 MPa and top surface 3-D visualization.

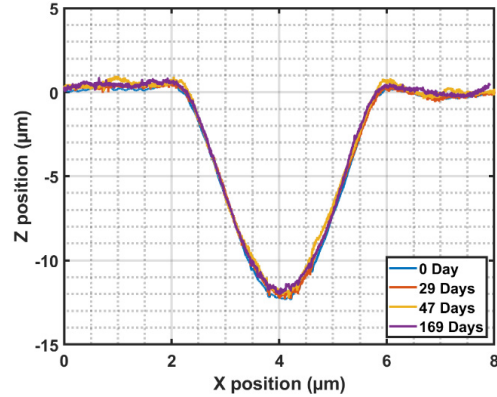


Fig. 11. Evolution of the diaphragm deflection in the sample sintered under 10 MPa over 169 days.

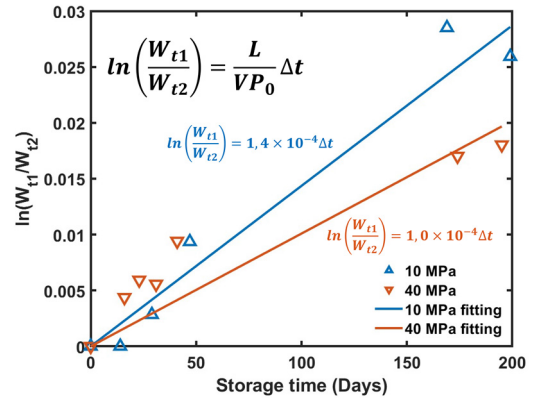


Fig. 12. Evolution of item $\ln(W_{t1}/W_{t2})$ with the storage time.

diaphragm has limited recovery over storage. The maximum deflection of the diaphragm changed from 12.3 μm on 0 days to 12.0 μm after 169 days.

Due to the diaphragm thickness variation, the deflection values of each sample varied. To calculate the leak rate of the package, the item $\ln(W_{t2}/W_{t1})$ of the samples sintered under 10 and 40 MPa was plotted in Fig. 12 as a function of the storage time. The data points fluctuate because of measurement inaccuracy. Furthermore, the linear fitting was calculated to evaluate the leak rate by using (2).

In this study, the cavity is assumed as a perfect cuboid, and the volume is accordingly calculated as 7.2×10^{-6} L. Subsequently, the leak rate is calculated as 1.2×10^{-12} and 8.4×10^{-13} $\text{Pa} \cdot \text{m}^3/\text{s}$. Thus, 10 and 40 MPa sintering pressure resulted in a reliable hermetic package. A lower leak rate was observed in the sample sintered under high

sintering pressure. It can be caused by the fewer pores in the sintered structure and a more solid connection between the metallization layer and the sintered sealing ring. The leak rate achieved in this study is considerably lower compared to the reported values of 10^{-11} to 10^{-9} Pa · m³/s achieved by the Ni/Sn solder bonding [23] and Au-Sn eutectic bonding [24] but still below the Cu thermos-compression enabled hermetic package as 10^{-17} Pa · m³/s [22]. However, this work achieved the comparable value as the reported sintered hermetic package of 10^{-14} Pa · m³/s [25] while implementing a longer storage and a smaller Cu sealing ring. Therefore, excellent hermeticity stability is demonstrated for the Cu nanoparticle sintering-enabled hermetic packages.

IV. CONCLUSION

This study demonstrates the successful hermetic sealing of an Si cavity using Cu nanoparticle sintering with a 50 μm sealing ring dimension. We demonstrate excellent bonding strength and hermetic stability. The following conclusions were obtained:

- 1) Hermetic sealing was achieved using thermos-compression bonding, with the boundary of the process parameter determined from 300 °C and 10 MPa. A strong shear strength of 280 MPa was obtained. According to the fracture surface analysis, stress concentration on the edge promoted the sintering. The fully sintered Cu in the surrounding area near the grooves contributed to the hermeticity.
- 2) A verified FEA model was established to evaluate the interior cavity pressure. The lowest value of 7 kPa was calculated. Additionally, robust hermetic stability was demonstrated over six months of storage. A low leak rate of 8.4×10^{-13} Pa · m³/s was extracted.

In future work, the role of the groove structure will be deeply investigated. In addition, on the one hand, an active device can be integrated to investigate the influence of the process on their performance. On the other hand, aging tests in extreme operation conditions should be conducted to evaluate the reliability performance.

ACKNOWLEDGMENT

The authors would like to thank the Delft University of Technology Else Kooi Laboratory staff for processing support and Henry Martin and Martien Kengen from Chip Integration Technology Center (CITC) for die shear tests.

REFERENCES

- [1] G. Q. K. Zhang, M. Graef, and F. van Roosmalen, "The rationale and paradigm of 'more than Moore,'" in *Proc. 56th Electron. Compon. Technol. Conf.*, 2006, pp. 151–157.
- [2] M. A. Schmidt, "Wafer-to-wafer bonding for microstructure formation," *Proc. IEEE*, vol. 86, no. 8, pp. 1575–1585, Aug. 1998.
- [3] C. S. Tan, J. Fan, D. F. Lim, G. Y. Chong, and K. H. Li, "Low temperature wafer-level bonding for hermetic packaging of 3D microsystems," *J. Micromech. Microeng.*, vol. 21, no. 7, Jul. 2011, Art. no. 075006.
- [4] M. M. Torunbalci, S. E. Alper, and T. Akin, "Wafer level hermetic sealing of MEMS devices with vertical feedthroughs using anodic bonding," *Sens. Actuators A, Phys.*, vol. 224, pp. 169–176, Apr. 2015.
- [5] A. Roshanghias, J. Bardong, and A. Binder, "Glass frit jetting for advanced wafer-level hermetic packaging," *Materials*, vol. 15, no. 8, p. 2786, Apr. 2022.
- [6] S.-H. Lee, J. Mitchell, W. Welch, S. Lee, and K. Najafi, "Wafer-level vacuum/hermetic packaging technologies for MEMS," *Proc. SPIE*, vol. 7592, Feb. 2010, Art. no. 759205.
- [7] C. M. Yang, H. Jung, J. H. Park, and H. Y. Kim, "Wafer-level reliability characterization for wafer-level-packaged microbolometer with ultra-small array size," *Microsyst. Technol.*, vol. 20, nos. 4–5, pp. 889–897, Apr. 2014.
- [8] A. Rautiainen, E. Österlund, H. Xu, and V. Vuorinen, "Mechanical characterization of bonded Au-Sn and Cu-Sn interconnections for MEMS packaging," in *Proc. Electron. Mater. Process. Packag. Space*, 2014, pp. 1–7.
- [9] Y. Takegawa, T. Baba, T. Okudo, and Y. Suzuki, "Wafer-level packaging for micro-electro-mechanical systems using surface activated bonding," *Jpn. J. Appl. Phys.*, vol. 46, no. 4B, pp. 2768–2770, Apr. 2007.
- [10] N. Malik, K. Schjølberg-Henriksen, E. Poppe, M. M. V. Taklo, and T. G. Finstad, "AlAl thermocompression bonding for wafer-level MEMS sealing," *Sens. Actuators A, Phys.*, vol. 211, pp. 115–120, May 2014.
- [11] S. Karlen, J. Haesler, T. Overstolz, G. Bergonzi, and S. Lecomte, "Sealing of MEMS atomic vapor cells using Cu-Cu thermocompression bonding," *J. Microelectromech. Syst.*, vol. 29, no. 1, pp. 95–99, Feb. 2020.
- [12] K. Mohan, N. Shahane, R. Liu, V. Smet, and A. Antoniou, "A review of nanoporous metals in interconnects," *JOM*, vol. 70, no. 10, pp. 2192–2204, Oct. 2018.
- [13] S. Takata, C. Chen, Y. Gao, and K. Suganuma, "Sintering Cu paste on Cu plates with different metallization," in *Proc. Int. Conf. Electron. Packag. (ICEP)*, 2019, pp. 1–6.
- [14] B. Zhang et al., "In-air sintering of copper nanoparticle paste with pressure-assistance for die attachment in high power electronics," *J. Mater. Sci., Mater. Electron.*, vol. 32, no. 4, pp. 4544–4555, Feb. 2021.
- [15] J. Li et al., "Low-temperature and low-pressure Cu-Cu bonding by highly sinterable Cu nanoparticle paste," *Nanos. Res. Lett.*, vol. 12, no. 1, pp. 1–6, Dec. 2017.
- [16] L. D. Carro, J. Zürcher, U. Drechsler, I. E. Clark, G. Ramos, and T. Brunswiler, "Low-temperature dip-based all-copper interconnects formed by pressure-assisted sintering of copper nanoparticles," *IEEE Trans. Compon., Packag., Manuf. Technol.*, vol. 9, no. 8, pp. 1613–1622, Aug. 2019.
- [17] M. Wiemer, F. Roscher, T. Seifert, K. Vogel, T. Ogashiwa, and T. Gessner, "Low temperature thermo compression bonding with printed intermediate bonding layers," *ECS Meeting Abstr.*, vol. MA2016–02, no. 32, p. 2106, Sep. 2016.
- [18] Y. Zhang, X. Li, Y. Mei, and G.-Q. Lu, "A novel hermetic sealing method for the metal package based on electric-current-assisted sintering of silver paste," *IEEE Trans. Compon., Packag. Manuf. Technol.*, vol. 11, no. 5, pp. 872–874, May 2021.
- [19] H. Zhang et al., "A new hermetic sealing method for ceramic package using nanosilver sintering technology," *Microelectron. Rel.*, vol. 81, pp. 143–149, Feb. 2018.
- [20] B. Zhang, Y. C. P. Carisey, A. Damian, R. H. Poelma, G. Q. Zhang, and H. W. van Zeijl, "3D interconnect technology based on low temperature copper nanoparticle sintering," in *Proc. 17th Int. Conf. Electron. Packag. Technol. (ICEPT)*, Aug. 2016, pp. 1163–1167.
- [21] A. Duan, K. Aasmundtveit, and N. Hoivik, "Ultra-low leak detection of Cu-Sn SLID for high density wafer level packaging," in *Proc. 12th Int. Conf. Electron. Packag. Technol. High Density Packag.*, Aug. 2011, pp. 1–4.
- [22] X. Wang, S. J. Bleiker, M. Antelius, G. Stemme, and F. Niklaus, "Wafer-level vacuum packaging enabled by plastic deformation and low-temperature welding of copper sealing rings with a small footprint," *J. Microelectromech. Syst.*, vol. 26, no. 2, pp. 357–365, Apr. 2017.
- [23] W. Yu-Chuan, Z. Da-Peng, X. Wei, and L. Luo, "Wafer-level hermetic package with through-wafer interconnects," *J. Electron. Mater.*, vol. 36, no. 2, pp. 105–109, Feb. 2007.
- [24] S.-H. Choa, "Reliability study of hermetic wafer level MEMS packaging with through-wafer interconnect," *Microsyst. Technol.*, vol. 15, no. 5, pp. 677–686, May 2009.
- [25] T. Ogashiwa et al., "Hermetic seal bonding at low-temperature with sub-micron gold particles for wafer level packaging," in *Proc. Int. Symp. Microelectron.*, Oct. 2015, vol. 2015, no. 1, pp. 73–78.